Near-infrared light propagation in an adult head model. I. Modeling of low-level scattering in the cerebrospinal fluid layer

Eiji Okada and David T. Delpy

Adequate modeling of light propagation in a human head is important for quantitative near-infrared spectroscopy and optical imaging. The presence of a nonscattering cerebrospinal fluid (CSF) that surrounds the brain has been previously shown to have a strong effect on light propagation in the head. However, in reality, a small amount of scattering is caused by the arachnoid trabeculae in the CSF layer. In this study, light propagation in an adult head model with discrete scatterers distributed within the CSF layer has been predicted by Monte Carlo simulation to investigate the effect of the small amount of scattering caused by the arachnoid trabeculae in the CSF layer. This low scattering in the CSF layer is found to have little effect on the mean optical path length, a parameter that can be directly measured by a time-resolved experiment. However, the partial optical path length in brain tissue that relates the sensitivity of the detected signal to absorption changes in the brain is strongly affected by the presence of scattering within the CSF layer. The sensitivity of the near-infrared signal to hemoglobin changes induced by brain activation is improved by the effect of a low-scattering CSF layer. © 2003 Optical Society of America

OCIS codes: 170.0170, 170.3660, 170.3890.

1. Introduction

Near-infrared spectroscopy (NIRS) and optical imaging are widely used to measure brain activation from the variation in intensity of detected light caused by alterations in cerebral oxygenation and hemodynamics. Light that propagates in the head is strongly scattered and the detected light travels considerably farther through the tissue than the physical length between the source and the detector. Adequate modeling of light propagation in the head to deduce the partial optical path length in the brain and the spatial sensitivity profile is important for quantitative NIRS[1,2] and optical imaging.[3–5] The heterogeneity of the tissues in the head, especially the nonscattering cerebrospinal fluid (CSF) that surrounds the brain, has been previously shown to have a strong effect on light propagation in the brain,[6–8] and hence the effects of a CSF layer cannot be ignored in any modeling of light propagation in the head. Since light tends to propagate in the shallow region of the inner skull table and the cerebral gray matter as a result of the influence of the CSF, the effect of nonsmoothness of the CSF boundary and the presence of small intrusions in the CSF layer on light propagation in the brain have also been investigated.[9,10] Although numerical analysis based on the diffusion approximation has been frequently applied to the modeling of light propagation in biological tissue, the diffusion approximation is not valid in a low-scattering region and the presence of the CSF layer prevents accurate modeling of light propagation in the head. Alternative attempts to examine the effect of including a low-scattering region in the head have relied on Monte Carlo models,[11] finite difference transport models,[12] or a hybrid radiosity finite-element model.[13,14]

In most previous studies,[6–14] a CSF layer has generally been modeled as a simple void structure such as an annular cavity filled with a clear nonscattering fluid. The anatomical structure of the CSF layer is in reality far more complex. The space between an arachnoid mater and a pia mater is filled with the CSF and fine arachnoid trabeculae extend across this

E. Okada (okada@elec.keio.ac.jp) is with the Department of Electronics and Electrical Engineering, Keio University, 3-14-1 Hiyoshi, Kohoku-ku, Yokohama 223-8522, Japan. D. T. Delpy is with the Department of Medical Physics and Bioengineering, University College London, 11-20 Capper Street, London WC1E 6JA, United Kingdom.

Received 13 September 2002; revised manuscript received 8 January 2003.

0003-6935/03/162906-09$15.00/0

gap from the arachnoid to the pia mater.[15] The light that propagates in the CSF layer is in practice likely to be scattered and absorbed by these arachnoid trabeculae.[16]

In this study, light propagation in adult head models with a CSF layer that incorporates various densities of discrete scatterers that mimic the arachnoid trabeculae has been predicted by Monte Carlo simulation to investigate the effect of low scattering in the CSF layer on the optical parameters measured in NIRS and optical imaging. The adult head model was a layered slab with a regular array of fine cylindrical discrete scatterers that modeled anisotropic scattering by the arachnoid trabeculae in the CSF layer. The mean optical path length for the adult forehead was also experimentally derived from time-resolved experiments and compared with the results from the model. The effect of low scattering in the CSF layer on the partial optical path length in the brain and the spatial sensitivity profile, optical parameters that are not directly obtainable experimentally were also derived from the results of the Monte Carlo simulation.

2. Parameters for Near-Infrared Spectroscopy Measurements

A. Mean Optical Path Length

The change in volume and oxygenation of blood that results from brain activation causes a variation in the absorption in the corresponding region of brain tissue. In common NIRS instruments, the change in intensity of the detected light is measured as a resulting signal. The detected light propagates considerably farther than the geometric distance between the source and the detector in biological tissue because of scattering, therefore a modified Beer–Lambert law has been used to obtain the relationship between the change in absorption coefficient $\Delta\mu_a$ in the tissue and the changes in the intensity of the detected light ΔOD.[17]

$$\frac{\Delta OD}{\Delta\mu_a} = \frac{\Delta \ln(I_0/I)}{\Delta\mu_a} \approx \langle L \rangle, \tag{1}$$

where I_0 is the intensity of incident light, I is the intensity of detected light, and $\langle L \rangle$ is the mean optical path length. Although OD is normally defined as the base 10 logarithmic ratio of the incident and the detected light intensity, in this paper we use a natural logarithm for all quantities to be consistent with other studies that use diffusion approximation. The change in the concentration of oxyhemoglobin and deoxyhemoglobin can be deduced from the change in absorption coefficient of several wavelengths. The mean optical path length can be obtained from time-resolved experiments with a pulsed laser and streak scope. Equation (1) is correctly valid only when the concentration of the absorber is homogeneously changed in the whole volume of tissue interrogated.

B. Partial Optical Path Length in the Brain

The absorption in the head is actually changed only locally during brain activation, and hence Eq. (1) is not strictly applicable for brain function measurements. Assuming that the head consists of several homogeneous tissue layers, a partial optical path length can be defined as an extension of the concept of the mean optical path length. The partial optical path length $\langle L_i \rangle$ is the mean optical path length that the detected light travels within a particular homogeneous region i. The change in intensity of the detected light can then be described by the sum of the product of the partial optical path lengths and the corresponding absorption coefficient change in each region.[18] The partial optical path length approximates a partial derivative of the change in the detected intensity versus absorption coefficient of each medium:

$$\frac{\partial OD}{\partial \mu_{ai}} \approx \langle L_i \rangle. \tag{2}$$

An absorption change in a particular region of tissue for which the partial optical path length is long would significantly contribute to the change in intensity of detected light. Hence, the partial optical path length indicates the sensitivity of the NIRS signal to absorption change in a particular part of the tissue. Although the total mean optical path length can be measured by the time-resolved experiment, the result of time-of-flight measurement contains no direct information about the partial optical path length that the light has traveled in each part of the tissue. In this study, the theoretically derived partial optical path length in the brain is used as an index of the sensitivity of the NIRS signal-to-brain activation, i.e., we assume that the absorption coefficient of the whole brain is homogeneously changed by brain activation. When the activated region in the brain is larger than the volume of tissue interrogated by a particular source–detector fiber pair, this assumption is correct and the absorption change caused by brain activation can be quantified by the change in intensity of detected light and the partial optical path length in the brain. However, the region of brain activation is often smaller than the volume of tissue interrogated, and hence the effective optical path length that the detected light travels in the activated region that contributes to the NIRS signal is shorter than the partial optical path length in the brain.

C. Spatial Sensitivity Profile

The partial optical path length in the brain indicates the sensitivity of the NIRS signal to absorption change in the brain tissue. However, the partial optical path length does not show the spatial distribution of the volume of tissue that contributes to the NIRS signal. The volume of tissue that contributes to the change in the intensity of the detected light can be obtained as the spatial sensitivity profile, which is calculated from the accumulated trajectories of the detected light.[19] The model is divided into voxels,

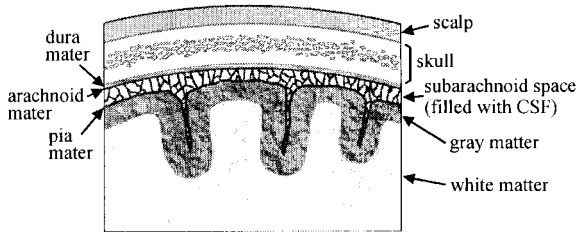

Fig. 1. Schematic diagram of the anatomical structure of the adult head.

and the mean partial optical path length that the detected light travels within each voxel $\langle L_{\text{voxel}}(x,y,z)\rangle$ can approximate the spatial sensitivity profile:

$$\frac{\partial OD}{\partial \mu_{a\ \text{voxel}}(x,y,z)} \approx \langle L_{\text{voxel}}(x,y,z)\rangle. \tag{3}$$

The spatial sensitivity profile cannot be obtained directly from experiments *in vivo*, although it is possible to measure this in simple homogeneous fluid phantoms.

3. Method

A. Adult Head Models

Figure 1 shows the schematic diagram of the cross section of an adult head. The superficial tissues of the brain have a layered structure that consists of the scalp, skull, dura mater, arachnoid mater, subarachnoid space filled with CSF, and pia mater. Brain is composed of gray matter and white matter. The simplified adult head model used for the prediction of the light propagation is a slab that consists of five layers that imitate the scalp, skull, CSF layer, gray matter, and white matter as shown in Fig. 2. In the head model, the dura mater, arachnoid mater, and pia mater were disregarded because they are appreciably thinner than the other layers. The thickness of each layer was decided on the basis of magnetic resonance imaging scans of adult foreheads. The optical properties of each layer for near-infrared light of 800-nm wavelength are listed in Table 1. They were chosen from reported data for dermis,[20] pig skull,[21] and human brain[22] measured *in vitro* by use of an integrating sphere system. In a previous study,[7] it was assumed that the CSF layer is an annular cavity filled with a nonscattering fluid, however, the anatomical structure of the CSF layer is in reality far more complex. The weblike strands known as the arachnoid trabeculae pass across the CSF layer between the arachnoid and the pia mater.[15] In this study, a regular array of fine cylindrical discrete scatterers of 0.1-mm diameter that extend perpendicularly from the skull to the gray matter were placed in the CSF layer to represent the low scattering produced by the arachnoid trabeculae. The rest of the space in the CSF layer was assumed to be filled with nonscattering CSF. Since the optical properties and density of arachnoid trabeculae were unknown, the optical properties of the discrete scatterers were assumed to be the same as those of the skull but anisotropic scattering was assumed. The scattering coefficient and the average cosine of the phase function of the discrete scatterers were 16 mm^{-1} and 0.9, respectively. The volume density of the discrete scatterers in the CSF layer was modeled for a range that varied from 0 to 50%. For the case when the density of the discrete scatterers is 20%, the

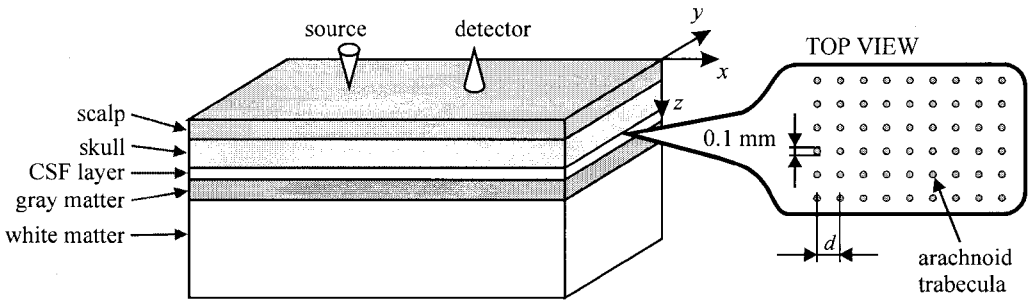

Fig. 2. Adult head model with discrete cylindrical scatterers in the CSF layer.

Table 1. Thickness and Optical Properties for Each Layer of the Adult Head Model

Tissue Type	Thickness (mm)	Transport Scattering Coefficient μ_s' (mm^{-1})	Absorption Coefficient μ_a (mm^{-1})
Scalp	3.0	1.9	0.018
Skull	7.0	1.6	0.016
Cerebrospinal fluid[a]	2.0	0.001	0.002
Arachnoid trabeculae[a]	—	$\mu_s = 16.0$ ($g = 0.9$)	0.016
Gray matter	4.0	2.2	0.036
White matter	—	9.1	0.014

[a]A regular array of arachnoid trabeculae is placed in the CSF layer and the rest of the space is filled with CSF.

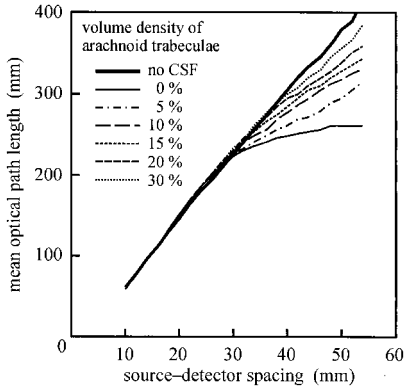

Fig. 3. Mean optical path length for the adult head model as a function of source–detector spacing predicted by Monte Carlo simulation.

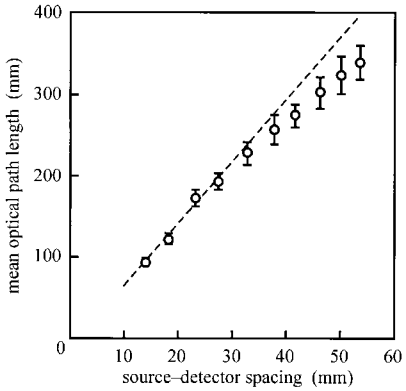

Fig. 4. Mean optical path length measured on the forehead of volunteers by time-resolved instrumentation. The broken line is a regression line obtained from results for source–detector spacings of less than 30 mm.

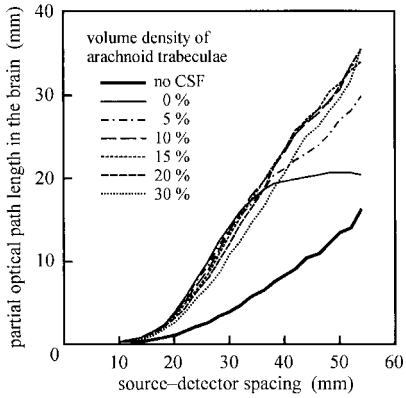

Fig. 5. Partial optical path length in the brain for the adult head model as a function of source–detector spacing predicted by Monte Carlo simulation.

spacing between the centers of the fine cylinders is 0.2 mm.

This sophisticated geometry in the CSF layer with the inclusion of quite a large number of fine cylindrical discrete scatterers considerably extended the computation time of the Monte Carlo simulation. For comparison, light propagation was also calculated for a simpler model in which the anatomical structure of the arachnoid trabeculae was totally ignored, but the optical properties of the CSF layer were changed to simulate the effect of the arachnoid trabeculae, i.e., uniform scattering was assumed. In this case, the transport scattering coefficient and absorption coefficient of the CSF layer were changed from $\mu_s' = 0.001$ to 0.8 mm^{-1} and from $\mu_a = 0.002$ to 0.009 mm^{-1}, respectively. Light propagation in the head model without a CSF layer was also calculated to investigate the effect of the low-scattering CSF layer on light propagation in the brain. In this latter head model, the CSF layer was replaced by the skull, and the depth of the brain from the surface of the head was the same as that for head models with the CSF layer.

B. Monte Carlo Simulation

Light propagation in the head model was calculated by use of a previously described Monte Carlo method[18] based on a variance reduction technique.[23,24] Reflection and refraction caused by refractive-index mismatch was considered only at the boundary between the scalp and the air. The mean optical path length and partial optical path length in the brain, which indicates the sensitivity of the detected near-infrared signal-to-brain activation, were calculated for each head model at source–detector spacings up to 55 mm. For the specific cases in which the light reached the detector at 30 or 40 mm from the source (distances typical of many NIRS studies), the trajectories of the detected light weighted by the detected intensity were accumulated to obtain the spatial sensitivity profiles. This enabled the partial optical path length that the detected light travels within each voxel $\langle L_{\mathrm{voxel}}(x, y, z)\rangle$ to be projected onto the plane perpendicular to the boundaries of the layers and along the source and detector (the x–z plane) and onto the plane parallel to the brain surface (the x–y plane). The partial optical path length within the voxels in the gray matter and white matter were only projected to obtain the spatial sensitivity profile in the x–y plane. Fifty million injected photons were traced for each head model.

C. Experimental Time-of-Flight Measurement of the Foreheads

The mean optical path length as a function of source–detector spacing was derived from time-resolved experiments in the reflection mode from adult foreheads of six volunteers. The light source was a Ti:sapphire pulsed laser that operates at 780 nm. Although this wavelength was 20 nm shorter than that used for the Monte Carlo simulation, the difference in the optical properties between two wavelengths would not cause a significant difference in light propagation in the head. The pulsed light was guided to the surface of the forehead by an optical fiber and the light that emerged from the head was collected into another optical fiber bundle and was detected with a streak scope for a range of source–detector spacings from 15 to 53 mm. The mean optical path length for each source–detector spacing was calculated from the measured temporal distribution of the detected light intensity.

4. Results and Discussion

A. Mean Optical Path Length for the Adult Head Model

The mean optical path length for the adult head models with various densities of discrete scatterers in the CSF layer is shown in Fig. 3. The mean optical path length for the head model without a CSF layer in-

creases almost linearly with increased source–detector spacing. The mean optical path length also depends on the density of discrete scatterers beyond source–detector spacings of 30 mm whereas the mean optical path length for all the head models is almost the same up to a source–detector spacing of 30 mm. The mean optical path length for the head model with the nonscattering CSF layer exhibits only a slow increase beyond a source–detector spacing of 30 mm. The slope of the relationship between the mean optical path length and the source–detector spacing increases with an increase in density of the discrete scatterers in the CSF layer. The relationship for the head models with the CSF layer that incorporates more than 50% discrete scatterers is almost identical to that for the head model without a CSF layer.

The mean optical path length for the foreheads of the six volunteers obtained from the time-resolved experiments is shown in Fig. 4. The dashed line is a regression line obtained from the experimental results for the source–detector spacing of less than 30 mm. The slope of the experimental results decreases slightly beyond a source–detector spacing of 30 mm. The experimental results most closely match those for the head model with a CSF layer that incorporates 15% discrete scatterers. In a previous study[7] it was assumed that the CSF layer is a nonscattering region, however, the tendency of the mean optical path length for the model with the nonscattering CSF layer is quite different from that obtained experimentally on adult foreheads. Although the geometry of the adult head model used here was much simpler than that of a real adult head, a good correlation between experimental and predicted data was obtained for a CSF layer that incorporates 10–20% discrete scatterers. To our knowledge there is no quantitative data about the density of the arachnoid trabeculae in human heads. Since the CSF can circulate in the subarachnoid space, a CSF layer that incorporates 10–20% discrete scatterers is a physiologically reasonable value and is similar to the volume occupied by the arachnoid trabeculae in anatomical sections.

B. Partial Optical Path Length in the Brain

The partial optical path length in the brain for the various models, which indicates the sensitivity of the NIRS signal to absorption change in the brain tissue, is shown in Fig. 5. The partial optical path length for all the models with a CSF layer starts to rise rapidly once the source–detector spacing exceeds 20 mm whereas the increase of that for the head model without a CSF layer is relatively slow. This indicates that a sandwich structure, in which there is a low-scattering CSF layer between the highly scattering skull and the gray matter, significantly affects the light propagation in the brain in an adult head. The sensitivity to absorption change in the gray matter is improved by the effect of the CSF layer. The partial optical path length for the models with a low-scattering CSF layer is almost the same as that for

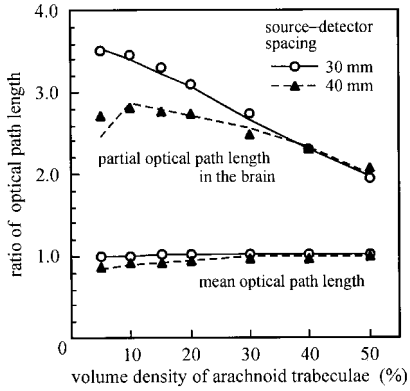

Fig. 6. Ratio of mean optical path length and partial optical path length in the brain for the adult head model with a low-scattering CSF layer to those for the model without a CSF layer as a function of volume density of the scatterers. The circles and triangles represent the results for the head model with the discrete scatterers in the CSF layer, and the curves represent the results for the simpler head model in which scattering is assumed to be homogeneous in the CSF layer.

the model with a nonscattering CSF layer in cases when the source–detector spacing is less than 35 mm. The partial optical path length for the model with a nonscattering CSF layer increases slowly beyond a source–detector spacing of 35 mm and levels off at 45 mm. Beyond a source–detector spacing of 35 mm, the slope of the relationship between the partial optical path length and the source–detector spacing increases when the density of the discrete scatterers in the CSF layer increases. The partial optical path length for the head models with a CSF layer that incorporates more than 10% discrete scatterers increases almost linearly with increased source–detector spacing. Figure 6 shows the ratios of the mean optical path length and the partial optical path length in the brain for the head models with low-scattering CSF layers to those for the head model without a CSF layer at source–detector spacings of 30 and 40 mm. The circles and triangles indicate the results for head models with discrete scatterers in the nonscattering CSF and the curves indicate the results for simpler head models with homogeneous scattering assumed in the CSF layer. The partial optical path length decreases with increased density of the discrete scatterers. However, the head models with a low-scattering CSF layer have approximately three times the partial optical path length in the brain compared with the model without the CSF layer. This indicates that the sensitivity of the NIRS signal-to-brain activation is improved by the presence of low scattering in the CSF layer.

The mean optical path length that can be measured by a time-resolved experiment is less affected by the presence of the low-scattering CSF layer. As can be seen in Fig. 3, the tendency of the mean optical path length for the models with a low-scattering CSF layer is more like that for a model without a CSF layer than that for a model with a nonscattering CSF layer. So for the calculation of this simple parameter it appears

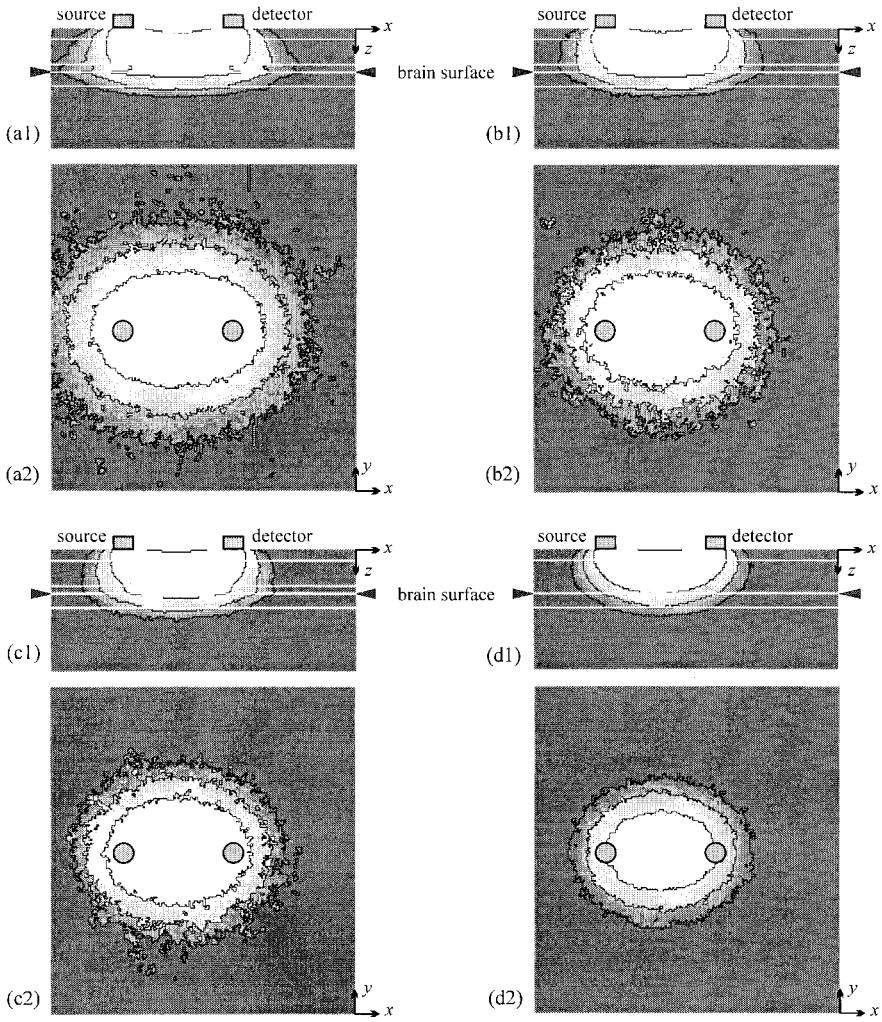

Fig. 7. Spatial sensitivity profiles in the x–z and x–y planes for a source–detector spacing of 30 mm. The model includes (a) a nonscattering CSF layer, (b) 10% volume density of scatterers in the CSF layer, (c) 20% volume density of scatterers in the CSF layer, (d) no CSF layer.

that the effect of the CSF layer could be disregarded. It should be noted, however, that the partial optical path length in the brain, which cannot be measured directly by the experiments, is highly affected by the presence of the low-scattering CSF layer. The presence of the CSF layer in the adult head model is thus important to obtain accurate predictions for light propagation in the brain.

The light propagation in the head model is affected by the optical properties of the brain. In this study we chose the optical properties of the adult brain from reported data measured *in vitro*.[22] It has also been reported that the scattering coefficients of the neonatal brain measured *in vitro*[22] and that of a child brain obtained by *in vivo* measurements[25] are lower than those used in our head model. A low-scattering coefficient for the brain increases the penetration depth of the detected light and partial optical path length in the brain, and the partial optical path length in the brain in a real adult head might be longer than that predicted by use of our head model.

In head models with discrete scatterers, we considered the spatial heterogeneity in the CSF layer caused by the arachnoid trabeculae and anisotropic scattering in the arachnoid trabeculae. Both the mean optical path length and the partial optical path length calculated for the models with discrete scatterers in the CSF layer are the same as those for the model that assumes a homogeneous scattering CSF layer. Since the detected light is highly scattered in the scalp, skull, and brain layers before and after it passes through the CSF layer, local heterogeneity and anisotropy in the CSF layer has only a slight effect on the light propagation and the direction of the arachnoid trabeculae in the real head is, of course, more irregular than that assumed in the head models. This result indicates that a simpler model, in which the anatomical structure of the arachnoid trabeculae is ignored but the optical properties of the homogeneous CSF layer are changed to incorporate the effects of the arachnoid trabeculae, is adequate to predict light propagation in head models. The

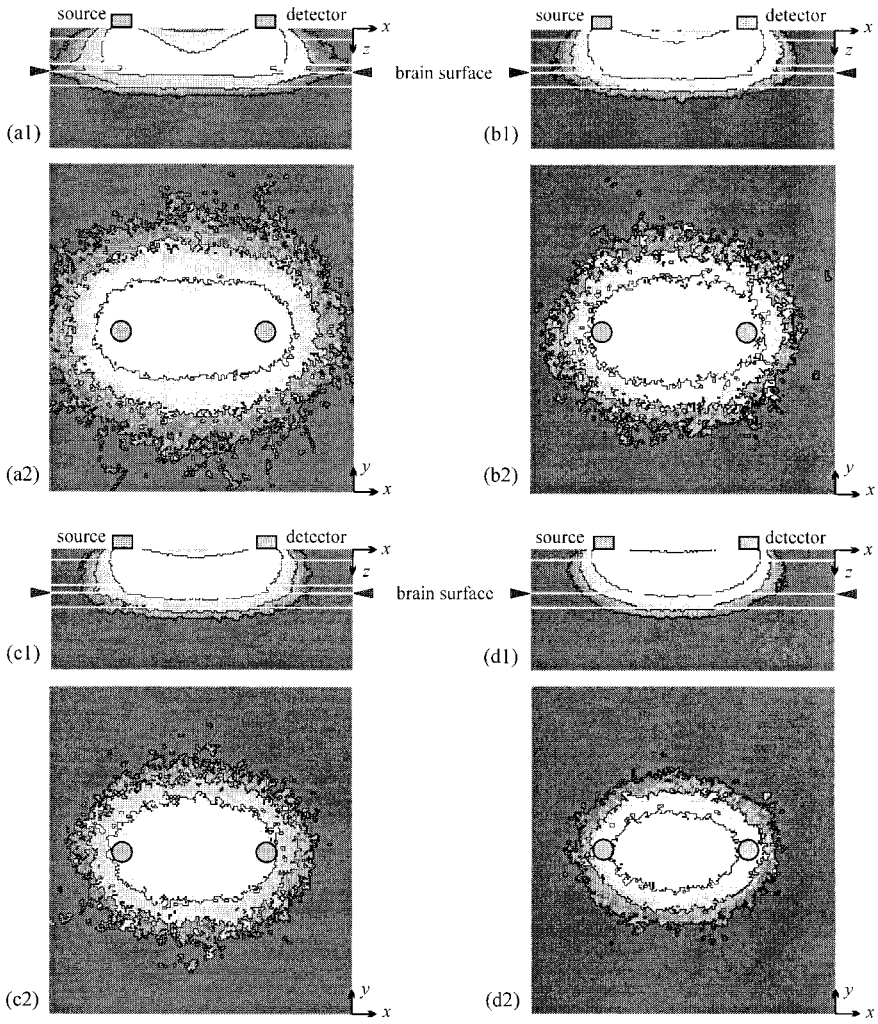

Fig. 8. Spatial sensitivity profiles in the x–z and x–y planes for a source–detector spacing of 40 mm. The model includes (a) a nonscattering CSF layer, (b) 10% volume density of scatterers in the CSF layer, (c) 20% volume density of scatterers in the CSF layer, (d) no CSF layer.

transport scattering coefficient that corresponds to the feasible volume density of discrete scatterers can range from 0.16 to 0.32 mm^{-1}.

C. Spatial Sensitivity Profile

The spatial sensitivity profiles in the x–z and x–y planes for the head models at a source–detector spacing of 30 mm are shown in Fig. 7. The spatial sensitivity profile for the head model with a nonscattering CSF is shown in Fig. 7(a) and those for the head models that incorporate 10% and 20% discrete scatterers in the CSF layer are shown in Figs. 7(b) and 7(c), respectively. For comparison Fig. 7(d) shows the spatial sensitivity profile for the head model without a CSF layer, where the spatial sensitivity profile in the x–z plane forms the well-known banana shape. The gray scale of all the profiles is normalized by the maximum value in Fig. 7(d). The contours in all the profiles are drawn for 10%, 1%, and 0.1% with respect to the maximum sensitivity point in Fig. 7(d). The spatial sensitivity profile in the head model with the nonscattering CSF shown in Fig. 7(a1) is obviously distorted around the CSF layer and shows a greater lateral spread through the gray matter as a result of the presence of the nonscattering CSF layer.

The most intense region of the spatial sensitivity profile in the x–y plane in all the models is located at the midpoint of the source and detector. In the model without the CSF, the first contour, which indicates the most sensitive region, is distributed around the midpoint of the source and detector as shown in Fig. 7(d2) whereas for the model with the nonscattering CSF layer it is broadly distributed around the source and detector as shown in Fig. 7(a2). However the penetration depth of the light into the brain tissue in both models is almost the same. The distortion of the spatial sensitivity profiles in the models with low scatterers in the CSF layer is reduced with an increase in the density of the scatterers. The comparison between mean optical path length obtained from the experiment and by the

Monte Carlo simulation indicates that the most likely volume density of the discrete scatterers in the CSF layer is from 10% to 20%. The spatial sensitivity profiles for the head model with 10% and 20% discrete scatterers are shown in Figs. 7(b) and 7(c), respectively. The distribution of the spatial sensitivity profiles in Figs. 7(b) and 7(c) are similar and the distributions are broader than those for the model without a CSF layer as shown in Fig. 7(d). The volume density of the discrete scatterers does not cause a significant difference in the spatial sensitivity profiles in the case of models with CSF layers that incorporate a physiologically feasible range of the density of discrete scatterers.

The equivalent spatial sensitivity profiles in the x–z and x–y planes in the head models at a source–detector spacing of 40 mm are shown in Fig. 8. These show a similar tendency for the change in spatial sensitivity profiles as was observed at a source–detector spacing of 30 mm. The sensitive region in the x–y plane in the brain in the head models that incorporate 10% and 20% discrete scatterers shown in Figs. 8(b) and 8(c) is broadly distributed between the source and the detector and hence the sensitive region is broadened with an increase in source–detector spacing. However, the penetration depth of the spatial sensitivity profile into brain tissue is not increased with an increase in source–detector spacing as shown in Figs. 8(b1) and 8(c1). As a result, the absorption change in the gray matter predominantly contributes to the NIRS signal.

5. Conclusion

The effect of low scattering caused by the arachnoid trabeculae in the CSF layer on light propagation in the brain has been investigated by Monte Carlo simulation. Although in practice the optical properties and density of the arachnoid trabeculae in the CSF layer are not known, it is feasible that the volume density might range from 10% to 20% in an adult head. The light propagation obtained for head models with discrete scatterers in the CSF layer is almost identical to those obtained for simpler head models whose scattering is assumed to be homogeneous in the CSF layer. The feasible range of the transport scattering coefficient for the CSF layer in this simpler model is from 0.16 to 0.32 mm^{-1}.

In these circumstances, at large source–detector spacing the mean optical path length for adult head models with a CSF layer is slightly shorter than that for a head model without a CSF layer whereas the partial optical path length in the brain for the model with the CSF layer is approximately three times as long as that for a model without a CSF layer. The partial optical path length cannot be directly measured whereas the mean optical path length can be obtained by time- or phase-resolved measurement. The results indicate that the sensitivity of the NIRS signal-to-absorption changes in the brain is clearly improved by the presence of a low-scattering CSF layer, although the signal is predominantly from cortical gray matter. The low-scattering CSF layer plays an important role in the light propagation in an adult head, and hence it is necessary to incorporate such a low-scattering CSF layer into adult head models for near-infrared spectroscopy and imaging.

The authors thank F. Kannari, N. Takei, K. Otsuka, and T. Tanabe at Keio University for their help with the time-resolved experiment, and H. Wabnitz and J. Steinbrink at Physikalisch-Technische Bundesanstalt and Y. Tsunazawa at Shimadzu Co., Ltd. for their informative suggestions. This research was partly supported by the Japan Society for the Promotion of Science, Grants-in-Aid for Scientific Research 13558116 and 13750397, a research grant from the Okawa Foundation for Information and Telecommunications, and a research grant from the Casio Science Promotion Foundation.

References

1. R. Springett, M. Wylezinska, E. B. Cady, M. Cope, and D. T. Delpy, "Oxygen dependency of cerebral oxidative phosphorylation in newborn piglets," J. Cereb. Blood Flow Metab. **20,** 280–289 (2000).
2. S. J. Matcher, C. E. Elwell, C. E. Cooper, M. Cope, and D. T. Delpy, "Performance comparison of several published tissue near-infrared spectroscopy algorithm," Anal. Biochem. **227,** 54–68 (1995).
3. J. C. Hebden, S. R. Arridge, and D. T. Delpy, "Optical imaging in medicine. I. Experimental techniques," Phys. Med. Biol. **42,** 825–840 (1997).
4. H. Koizumi, Y. Yamashita, A. Maki, T. Yamamoto, Y. Ito, H. Itagaki, and R. Kennan, "Higher-order brain function analysis by trans-cranial dynamic near-infrared spectroscopy imaging," J. Biomed. Opt. **4,** 403–413 (1999).
5. B. Chance, E. Anday, S. Nioka, S. Zhou, L. Hong, K. Worden, C. Li, T. Murray, Y. Ovetsky, D. Pidikiti, and R. Thomas, "A novel method for fast imaging of brain function, noninvasively, with light," Opt. Express **2,** 411–423 (1998), http://www.opticsexpress.org.
6. M. Firbank, S. R. Arridge, M. Schweiger, and D. T. Delpy, "An investigation of light transport through scattering bodies with nonscattering regions," Phys. Med. Biol. **41,** 767–783 (1996).
7. E. Okada, M. Firbank, M. Schweiger, S. R. Arridge, M. Cope, and D. T. Delpy, "Theoretical and experimental investigation of near-infrared light propagation in a model of the adult head," Appl. Opt. **36,** 21–31 (1997).
8. M. Wolf, M. Keel, V. Dietz, K. von Siebenthal, H. U. Bucher, and O. Baenziger, "The influence of a clear layer on near-infrared spectrophotometry measurements using a liquid neonatal head phantom," Phys. Med. Biol. **44,** 1743–1753 (1999).
9. H. Dehghani and D. T. Delpy, "Near-infrared spectroscopy of the adult head: effect of scattering and absorbing obstructions in the cerebrospinal fluid layer on light distribution in the tissue," Appl. Opt. **39,** 4721–4729 (2000).
10. J. Ripoll, N. Nieto-Vesperinas, S. R. Arridge, and H. Dehghani, "Boundary conditions for light propagation in diffuse media with nonscattering regions," J. Opt. Soc. Am. A **17,** 1671–1681 (2000).
11. K. Uludag, M. Kohl, J. Steinbrink, H. Obrig, and A. Villringer, "Cross talk in the Lambert–Beer calculation for near-infrared wavelength estimated by Monte Carlo simulation," J. Biomed. Opt. **7,** 51–59 (2002).
12. A. H. Hielscher, R. E. Alcuffe, and R. L. Barbour, "Comparison of finite-difference transport and diffusion calculations for photon migration in homogeneous and heterogeneous tissue," Phys. Med. Biol. **43,** 1285–1302 (1998).
13. M. Firbank, E. Okada, and D. T. Delpy, "A theoretical study of

the signal contribution of regions of the adult head to near-infrared spectroscopy studies of visual evoked responses," Neuroimage **8,** 69–78 (1998).
14. S. R. Arridge, H. Dehghani, M. Schweiger, and E. Okada, "The finite element model for the propagation of light scattering media: a direct method for domain with nonscattering regions," Med. Phys. **27,** 252–264 (2000).
15. M. B. Carpenter and J. Sutin, *Human Neuroanatomy* (Williams & Wilkins, Baltimore, Md., 1983).
16. E. Okada and D. T. Delpy, "Investigation of the effect of discrete scatterers in CSF layer on optical path length in the brain," in *Photon Migration, Diffuse Spectroscopy, and Optical Coherence Tomography: Imaging and Functional Assessment*, S. Andersson-Engels and J. G. Fujimoto, eds., Proc. SPIE **4160,** 196–203 (2000).
17. D. T. Delpy, M. Cope, P. van der Zee, S. R. Arridge, S. Wray, and J. Wyatt, "Estimation of optical pathlength through tissue from direct time of flight measurement," Phys. Med. Biol. **33,** 1433–1442 (1988).
18. M. Hiraoka, M. Firbank, M. Essenpreis, M. Cope, S. R. Arridge, P. van der Zee, and D. T. Delpy, "A Monte Carlo investigation of optical pathlength in inhomogeneous tissue and its application to near-infrared spectroscopy," Phys. Med. Biol. **38,** 1859–1876 (1993).
19. E. Okada, M. Firbank, and D. T. Delpy, "The effect of overlying tissue on the spatial sensitivity profile of near-infrared spectroscopy," Phys. Med. Biol. **40,** 2093–2108 (1995).
20. C. R. Simpson, M. Kohl, M. Essenpreis, and M. Cope, "Near-infrared optical properties of *ex vivo* human skin and subcutaneous tissue measured using the Monte Carlo inversion technique," Phys. Med. Biol. **43,** 2465–2478 (1998).
21. M. Firbank, M. Hiraoka, M. Essenpreis, and D. T. Delpy, "Measurement of the optical properties of the skull in the wavelength range 650–950 nm," Phys. Med. Biol. **38,** 503–510 (1993).
22. P. van der Zee, M. Essenpreis, and D. T. Delpy, "Optical properties of brain tissue," in *Photon Migration and Imaging in Random Media and Tissues*, R. R. Alfano and B. Chance, eds., Proc. SPIE **1888,** 454–465 (1993).
23. B. C. Wilson, "A Monte Carlo model for the absorption and flux distribution of light in tissue," Med. Phys. **10,** 824–830 (1983).
24. P. van der Zee and D. T. Delpy, "Simulation of the point spread function for light in tissue by a Monte Carlo technique," Adv. Exp. Med. Biol. **215,** 179–191 (1987).
25. F. Bevilacqua, D. Piguet, P. Marquet, J. D. Gross, B. J. Tromberg, and C. Depeursinge, "*In vivo* local determination of tissue optical properties: applications to human brain," Appl. Opt. **38,** 4939–4950 (1999).